Probing nanoscale graphene-liquid interfacial interactions via Ultrasonic Force Spectroscopy

Supplementary Information

Benjamin J. Robinson and Oleg V. Kolosov

Physics Department, Lancaster University, Lancaster, LA1 4YB, UK

Supplementary Note 1: Ultrasonic Force Spectroscopy (UFS) operating principle

In UFS measurements the sample is vibrated in the oscillating (harmonic) way at high frequency (HF) well above free cantilever free and contact resonances. Due to the extreme dynamical rigidity of the cantilever the vibration of the sample is not transferred to the cantilever and therefore one can safely assume that the tip-surface distance is also oscillated at the same ultrasonic frequency f and the amplitude a. Due to the highly nonlinear dependence of the interaction force on the tip-surface distance[1, 2] such oscillation is "rectified" producing an additional "ultrasonic" force that can be defined as a function $F_m(h_1, a)$ dependent on the initial indentation h_1, the ultrasonic amplitude a and original force-vs-distance dependence in the absence of the ultrasonic vibration $F(h)$. The new force F_m can be calculated as follows:

$$F_m(h_1, a) = \frac{1}{T}\int_T F[h_1 - a\cos(2\pi ft)]dt$$

where $F(h)$ is the force dependence on the indentation depth without ultrasonic vibration and the integral is taken over a period $T = 1/f$. The initial cantilever deflection z_0 is defined by set force $F_0 = k_c z_0$ where k_c is the cantilever spring constant, however the additional ultrasonic force leads to an additional cantilever deflection z_a such that new equilibrium position of the cantilever $z = z_0 + z_a$

Supplementary Note 2: Relationship between the nonlinear UFS response and force-vs-indentation dependence.

In order to effectively detect z_a, which depends on the effective Young's modulus of the specimen and probe,[3] the HF ultrasonic vibration is modulated using a gated saw-tooth signal at low frequency (LF), typically 1 – 3 KHz (Fig. S1b). The resulting low frequency (LF) cantilever vibrations are detected with high resolution by a lock-in amplifier, yielding RMS amplitude that is recorded as the UFM (nanomechanical) signal accompanied by simultaneous acquisition of topography maps. Fig. S1 shows schematically the acquisition of the UFM nonlinear response z_a for a typical force vs indentation relation (Fig. S1a) with ultrasonic amplitude of a = 1 nm.

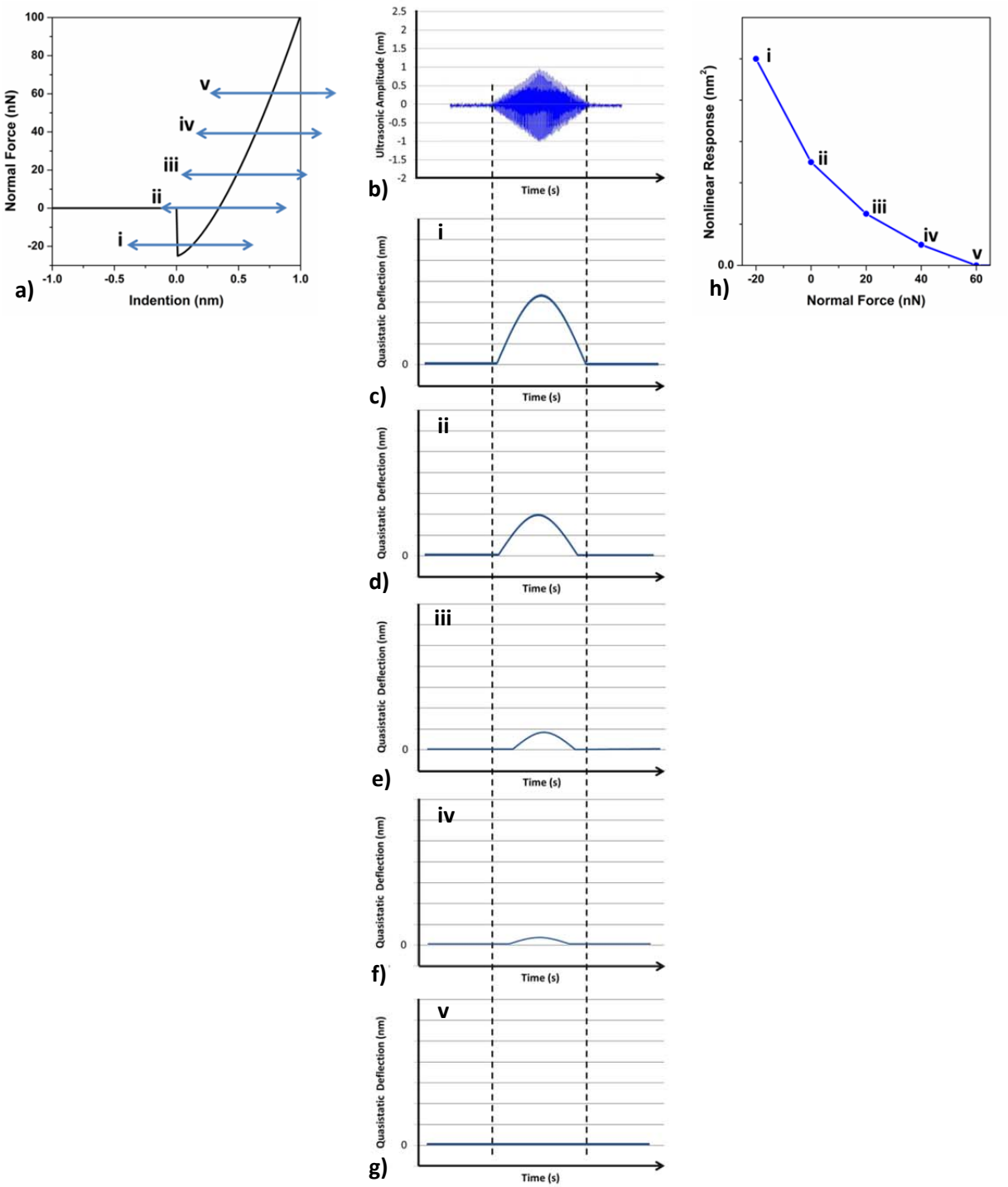

Fig S1. Schematic representation, during UFM operation, of a) normal force vs indentation where arrows i-v show the ultrasonic oscillations of a = 1 nm at discreet forces. b) triangular LF envelope of HF vibration and c-g) UFM quasistatic deflection of the cantilever z_a corresponding to forces at points i-v as acquired by lock-in amplifier (note that vertical black dashed lines are guide to eye only). h) shows the relative magnitudes of the nonlinear response (area under quasistaic deflection curves) until *a* is insufficient to overcome the linear region of indentation (point v) and nonlinear response is zero.

Fig. S2 shows the modified force curve $F_m(h_1, a)$, calculated using the DMT contact mechanics model without an explicit liquid layer, hence no hydration force component. As

the ultrasonic amplitude increases from 0 to 1 nm, we note that the model predicts a decrease in the magnitude of adhesion (negative normal force) which was confirmed experimentally (see force curves in Fig. S6 below).

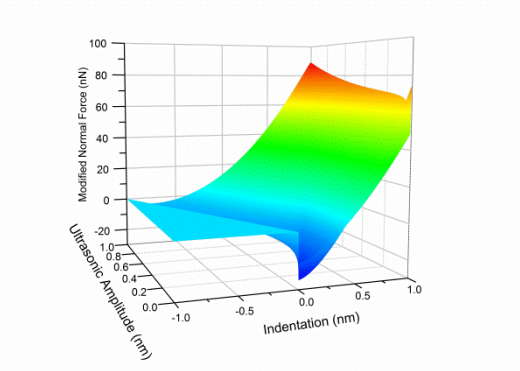

FIG S2. Calculated plot showing the modified normal force-vs-indentation relationship due to UFM ultrasonic oscillation of increasing amplitudes. Here we assume a sample effective Young's modulus of *E*=75 GPa and cantilever & tip parameters described in table 2 without a liquid environment.

Supplementary note 3: Theoretical analysis of sensitivity of simulated UFS response.

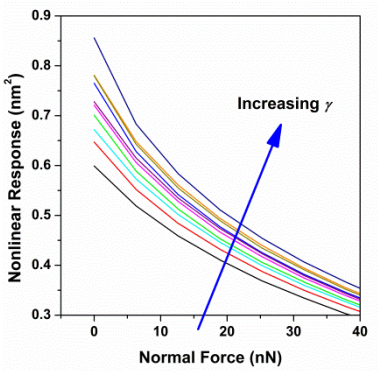

Fig S3. Theoretical analysis of sensitivity of UFS with incrementally increasing value of γ_{sample} in the range 0.05 – 0.50 Jm^{-2} and 0.05 Jm^{-2} steps.

Fig. S3 shows the theoretical analysis of dependence of UFS response on the effective surface energy for a material with fixed E = 35 GPa, and γ_{sample} is incremented in 0.05 Jm^{-2} steps from 0.05 to 0.50 Jm^{-2}.

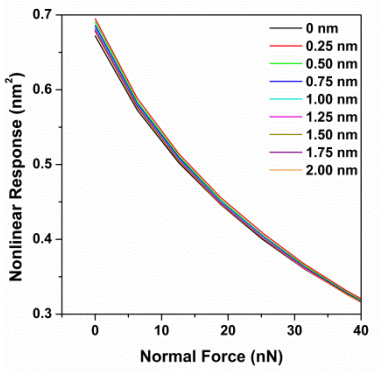

Fig S4. Theoretical analysis of sensitivity of UFS for a system with E_{sample} = 35 GPa with incrementally increasing value of λ_{liquid} in the range 0 to 2 nm in 0.25 nm steps

Fig. S4 shows the theoretical analysis of relation between UFS response and water decay length for a stiff material with fixed E = 35 GPa, and λ_{liquid} in the range 0 to 2 nm in 0.25 nm steps.

Supplementary Note 4: Force-vs-separation curves and UFS nonlinear response curves in various environments.

Fig. S5 shows experimentally obtained UFS response and simultaneously captured force-vs-separation (force spectroscopy) data for FLG in air, water and dodecane environments at a range of ultrasonic amplitudes (*a*). Fig. S6 shows comparable data for SiO_2 captured at the same ultrasonic amplitude.

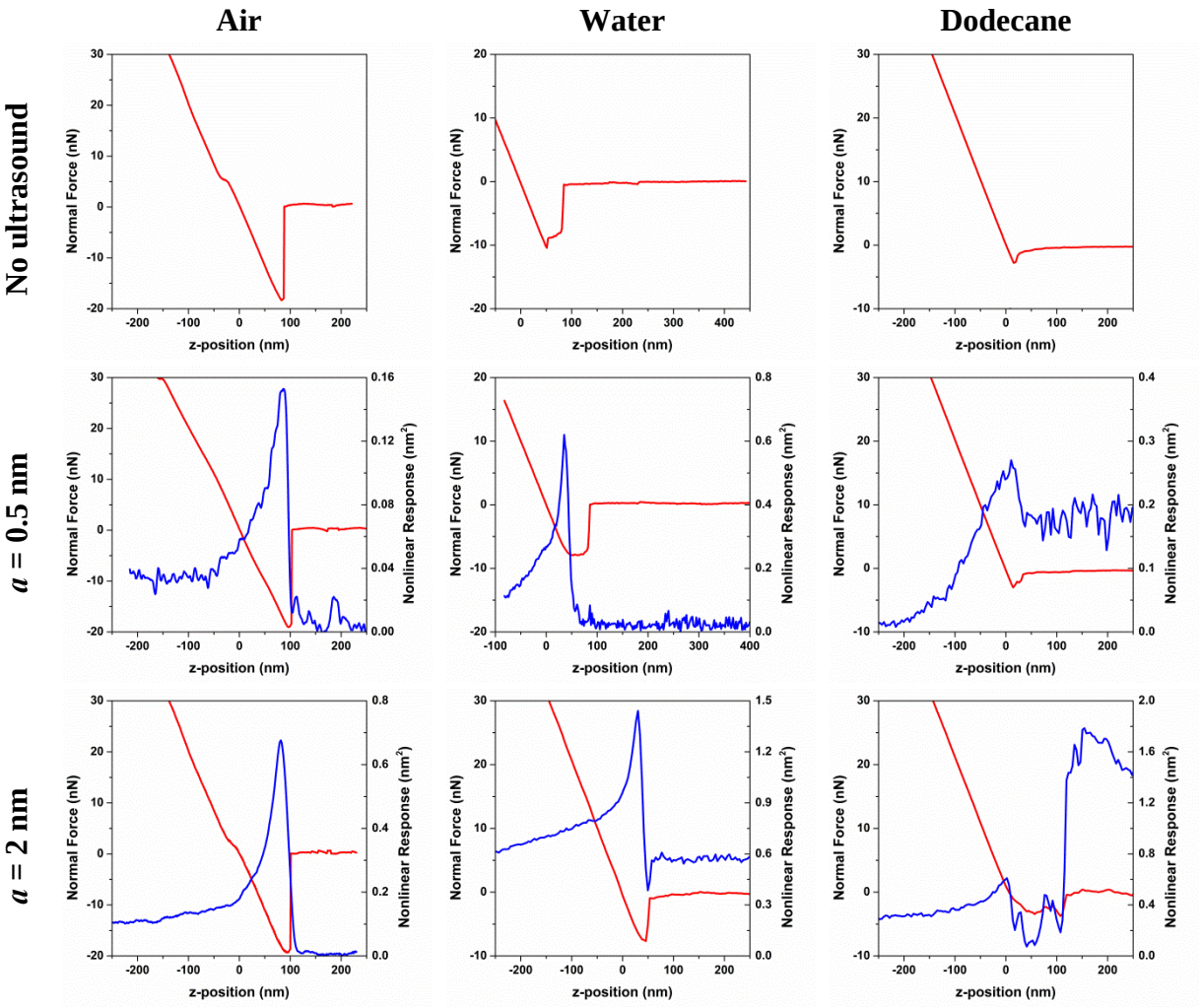

Fig S5. Typical experimentally obtained UFS response (blue) and normal force (red) for FLG for the retraction branch of the approach-retract curves in air, water and dodecane at ultrasonic amplitudes of 0, 0.5 and 2 nm.

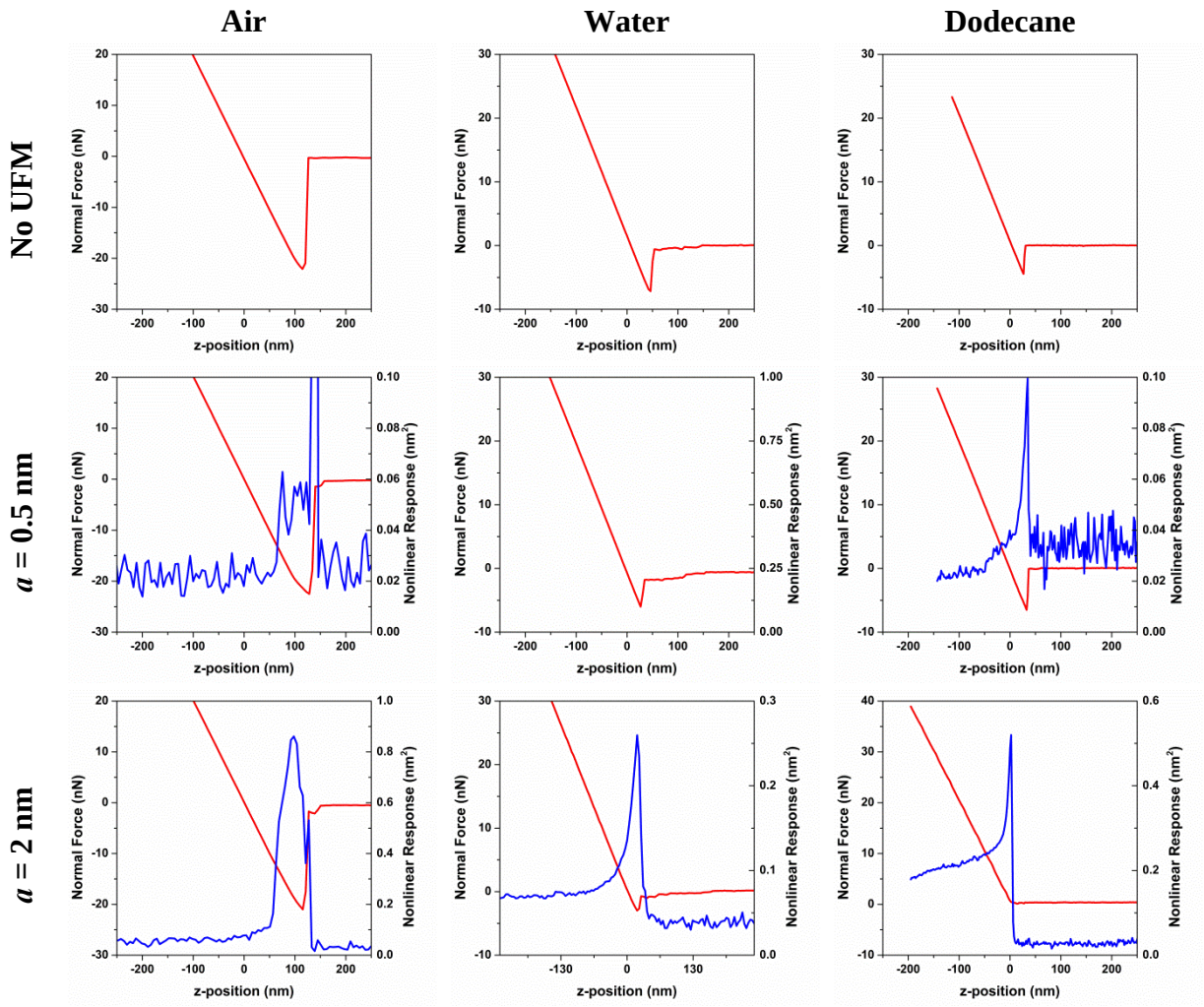

Fig S6. Typical experimentally obtained UFS response (blue) and normal force (red) for SiO_2 for the retraction branch of the approach-retract curves in air, water and dodecane at ultrasonic amplitudes of 0, 0.5 and 2 nm.

Non-zero, UFS response at distances far from the surface in both liquid environments is most likely due to acoustic pressure acting on the cantilever which is suppressed during the period of solid-solid contact when the dominant response is that arising from the probe-sample interface. This can be observed, for example, for the FLG response at a = 0.5 nm in dodecane, where the UFS signal is in some parts lower during the solid-solid contact than during no probe-sample contact. For measurement of UFS as shown in Figs 2, 3 and 4 of the main paper, only nonlinear response corresponding to the solid-solid contact regions was considered.

Supplementary Note 5: Complete FLG flake image

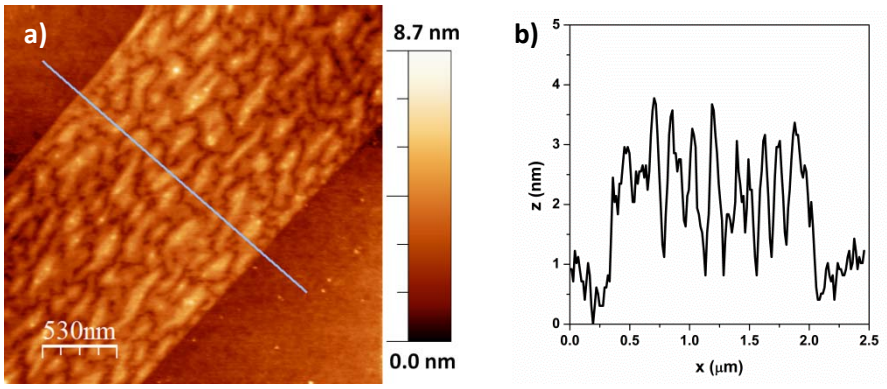

Fig S7. a) Contact mode AFM topography showing the full width of the FLG flake on SiO_2 substrate and b) corresponding profile of corrugated FLG surface.

Supplementary Note 6: Comparison of contact, tapping and UFM imaging modes on graphene structures

Graphene grown by the carbon diffusion technique, previously reported,[4] results in complex films comprising both Pt supported and delaminated (suspended) regions and as such provide an excellent comparison of the relative information provided by different SPM modes. In Fig S8 we show similar areas of the film investigated by tapping mode (topography and phase) and contact/UFM mode (topography and nonlinear response).

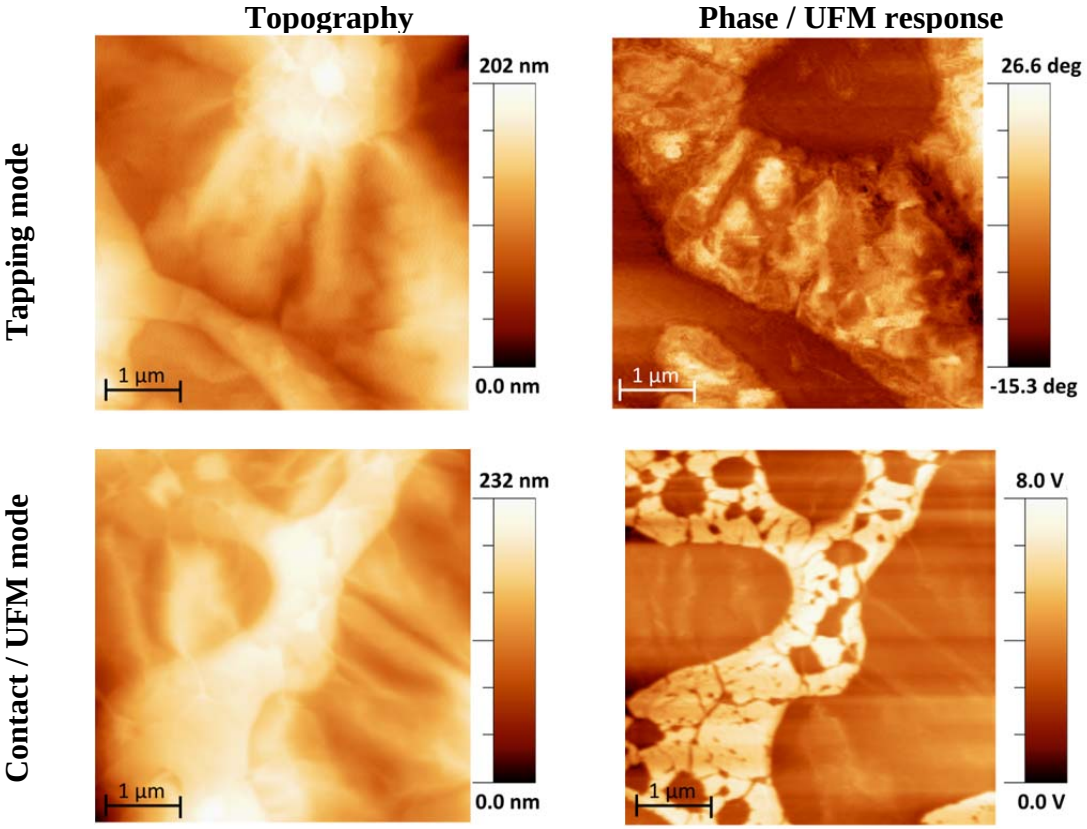

Fig S8. Examples of a) Topography and b) phase of supported and suspended FLG film and c) topography and d) UFM nonlinear response.

We note that there is a negligible difference in the degree of information provided by the topography images of both modes. Whilst, the phase response of tapping mode provides some information concerning the mechanics of the films, the UFM response is less ambiguous and, in general, clearer to interpret.

Supplementary Note 7: Effect of $\gamma_{graphene}$ on the fitting of theoretical response ratio to experimental data

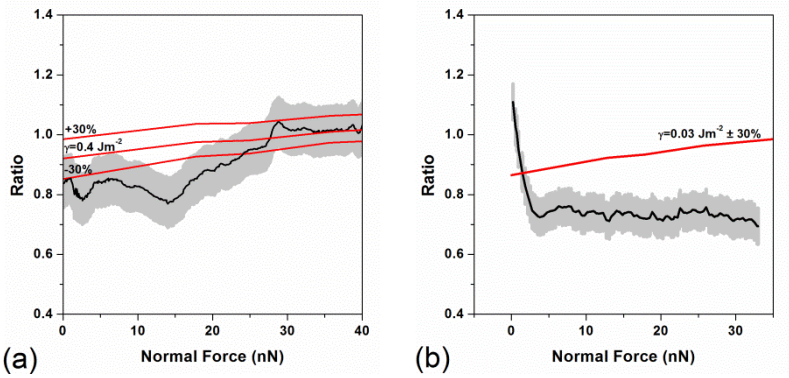

Fig S9. Comparison of FLG and SiO_2 experimental (black) and theoretical (red) nonlinear response ratios at a = 2 nm with variation of FLG Youngs modulus in a) ambient conditions and b) dodecane environment. The grey region represents the associated uncertainty for the experimental responses.

1. F. Dinelli, S. K. Biswas, G. A. D. Briggs and O. V. Kolosov, *Physical Review B*, 2000, **61**, 13995-14006.
2. F. Dinelli, M. R. Castell, D. A. Ritchie, N. J. Mason, G. A. D. Briggs and O. V. Kolosov, *Philosophical Magazine A, Physics of Condensed Matter Structure Defects and Mechanical Properties*, 2000, **80**, 2299-2323.
3. O. V. Kolosov, I. Grishin and R. Jones, *Nanotechnology*, 2011, **22**, 8.
4. B. J. Robinson, C. Rabot, R. Mazzocco, A. Delamoreanu, A. Zenasni and O. V. Kolosov, *Thin Solid Films*, 2014, **550**, 472-479.